HHS Public Access

Author manuscript

*Gastroenterology*. Author manuscript; available in PMC 2023 June 01.

Published in final edited form as:

*Gastroenterology*. 2022 June ; 162(7): 2047–2062. doi:10.1053/j.gastro.2022.02.035.

# IRAK4 signaling drives resistance to checkpoint immunotherapy in pancreatic ductal adenocarcinoma

**Vikas Somani**[1,§], **Daoxiang Zhang**[1,3,§], **Paarth B. Dodhiawala**[1], **Varintra E. Lander**[1], **Xiuting Liu**[1], **Liang-I Kang**[1,2], **Hung-Po Chen**[1], **Brett L. Knolhoff**[1], **Lin Li**[1], **Patrick M. Grierson**[1], **Mariana B. Ruzinova**[2], **David G. DeNardo**[1], **Kian-Huat Lim**[1,*]

[1]Division of Oncology, Department of Internal Medicine, Barnes-Jewish Hospital and The Alvin J. Siteman Comprehensive Cancer Center, Washington University School of Medicine, St. Louis, MO 63110

[2]Department of Pathology and Immunology, Barnes-Jewish Hospital and The Alvin J. Siteman Comprehensive Cancer Center, Washington University School of Medicine, St. Louis, MO 63110

[3]Current address: School of Life Science, Anhui Medical University, Anhui, China

## Abstract

**Background and Aims:** Checkpoint immunotherapy is largely ineffective in pancreatic ductal adenocarcinoma (PDAC). The innate immune NF-κB pathway promotes PDAC cell survival, stromal fibrosis and is driven by IRAK4, but its impact on tumor immunity has not been directly investigated.

**Methods:** We interrogated the TCGA data to identify the correlation between NF-κB and T cell signature, and a PDAC tissue microarray (TMA) to correlate IRAK4 activity with $CD8^+$ T cells abundance. We performed RNAseq on *IRAK4*-deleted PDAC cells, and single cell RNAseq on autochthonous KPC (*p48-Cre/TP53*$^{fl/f}$/*LSL-KRAS*$^{G12D}$) mice treated with an IRAK4 inhibitor. We generated conditional *IRAK4*-deleted KPC mice and complementarily used IRAK4 inhibitors to determine the impact of IRAK4 on T cell immunity.

**Results:** We found positive correlation between NF-κB activity, IRAK4 and T cell exhaustion from TCGA. We observed inverse correlation between phosphorylated IRAK4 and $CD8^+$ T cell abundance in a PDAC TMA. Loss of *IRAK4* abrogates NF-κB activity, several immunosuppressive factors, checkpoint ligands and hyaluronan synthase 2 (HAS2), all of which drive T cell dysfunction. Accordingly, conditional deletion or pharmacologic inhibition of IRAK4 markedly decreased tumor desmoplasia and increased the abundance and activity of infiltrative $CD4^+$ and $CD8^+$ T cells in KPC tumors. Single cell RNAseq showed myeloid and fibroblast reprograming towards acute inflammatory responses following IRAK4 inhibition. These changes set the stage for successful combination of IRAK4 inhibitors with checkpoint immunotherapy, resulting in excellent tumor control and markedly prolonged survival of KPC mice.

*Corresponding author: Kian-Huat Lim, Washington University School of Medicine, 660 South Euclid Avenue, Campus Box 8069, Saint Louis, MO 63110, Tel: 314-362-6157, Fax: 314-747-9329, kian-huat.lim@wustl.edu.

§These authors contributed equally

the authors have declared no conflict of interests.

**Conclusion:** IRAK4 drives T cell dysfunction in PDAC and is a novel, promising immunotherapeutic target.

### Keywords

CA-4948; NF-κB; T cell exhaustion; HAS2; PD-L1

## INTRODUCTION

Chronic inflammation fuels PDAC progression, treatment resistance and T cell dysfunction in pancreatic ductal adenocarcinoma (PDAC)[1]. A major molecular mechanism that drives inflammation is engagement of the innate Toll-like (TLRs) and IL-1 receptors. In mouse models, caerulein-induced pancreatitis and progression to PDAC is dependent on TLR7 and TLR9[2, 3]. In a *KRAS*$^{G12D}$-driven genetically engineered mouse model (GEMM), IL-1α-IKK-NF-kB signaling is absolutely required for PDAC development[4]. The TLRs and IL-1R are sentinel receptors that sense danger signals and trigger innate and adaptive immune responses. Ligation of TLR/IL-1Rs recruits the adaptor protein MyD88 and Interleukin-1 Receptor Associated Kinase-4 (IRAK4), which signals through TAK1 to activate the IKK-NF-kB, p38/MAPK, and type-1 interferon pathways[5], ultimately leading to enhanced cell survival and secretion of cytokines and chemokines that draw inflammatory cells. In PDAC, phospho-activated IRAK4 staining strongly correlates with activated RELA, a key canonical NF-κB transcription factor, and poor survival[6]. IRAK4 can be activated by IL-1R and TLR9 receptors as part of the inflammatory network triggered by oncogenic *KRAS* and genotoxic stress[7]. Accordingly, suppression of IRAK4 impairs *KRAS*-induced tumorigenesis, stromal fibrosis and chemo-resistance[6, 8]. Moreover, NF-κB activity in pancreatic stellate cells reduces T cell infiltration via secretion of CXCL12[9]. However, the impact of tumor NF-κB signaling on immune resistance in PDAC has not been directly investigated.

## MATERIAL and METHODS (Additional information in Supplementary Data)

### Mouse strains and cell lines

IRAK4 targeting vector and *IRAK4*$^{fl/WT}$ mice were generated by Ingenious targeting laboratory. Briefly, exons 2–12 of *IRAK4* were flanked by LoxP sites and split GFP cassettes. This stage was designed to express as wild-type with no GFP expression. Cre-mediated deletion of exons 2–12 resulted in near-complete deletion of the *IRAK4*-coding region. After the Cre-mediated recombination event, the two GFP cassette come together and express under the CAG promoter on the antisense strand. The neomycin selection cassette is removed at the embryonic stem (ES) cell stage via Ingenious' proprietary FLP ES cells with no additional electroporation or mating required. Homozygous *IRAK4*$^{fl/f}$ were generated and crossed into *p48-Cre*/*TP53*$^{fl/f}$ and *TP53*$^{fl/f}$/*LSL-KRAS*$^{G12D}$ mice to generate *p48-Cre*/*TP53*$^{fl/f}$/*IRAK4*$^{fl/f}$ and *TP53*$^{fl/f}$/*LSL-KRAS*$^{G12D}$/*IRAK4*$^{fl/f}$ parents, which were crossed to generate *IRAK4*$^{fl/f}$ KPC mice. *IRAK4*-null mice were purchased from EUCOMM and genotyped as recommended[10]. Nur77-GFP (C57BL/6-Tg(Nr4a1-EGFP/cre)820Khog/J) mice were purchased from Jackson Laboratories and genotyped as recommended.

### Immunohistochemistry (IHC), immunofluorescence (IF) and quantification

IHC and IF staining protocol and antibodies were described in Supplementary Data and Supplementary Table 2. Quantification was performed in blinded manner using HALO or ImageJ software.

### Xenograft tumorigenesis assay

C57BL/6J and FVB/NJ mice were purchased from the Jackson Laboratories. Autochthonous KPC breeding pairs were a gift from David DeNardo and genotyped as published[11]. For subcutaneous and orthotopic inoculation, approximately 5 million cells or 100 thousand cells, respectively were implanted into 6~8-week-old mice. Drug treatment was initiated when tumors were palpable. Drug dosing, frequent and route of administration were provided in Supplementary Data Table 2.

### Flow cytometry analysis

Data acquisition was performed on the BDX2 (BD Biosciences), and Flow Jo X 10.0.7r2 (Tree Star) was used for analysis with appropriate compensation. Gating strategies were demonstrated in Supplementary Figure 8. All antibodies used for flow cytometry are listed in Supplementary Table 1.

### Statistical analyses

Statistical analysis was performed using the GraphPad Prism 8 software. Unpaired student's two-tailed t-tests were used to compare two groups when appropriate. For multiple groups, one-way or two-way ANOVA analysis with appropriate post-tests were used. In instances of systemic/group variation, repeated measures ANOVA was utilized. Unadjusted $P < .05$ were considered as statistically significant. Adjusted $P$ value metrics are stated at end of each figure legend where applicable. Kaplan-Meier curves were generated analysed by log-rank tests.

### Study approvals and data availability

The Washington University PDAC Tissue Micro-Array (TMA) was IRB approved (#201404143) and published[12]. Patient consent was waived per IRB approval. All studies were performed per ethical principles of Declaration of Helsinki. All mouse experiments were conducted under IACUC approval (#20190138). RNAseq data is deposited in GEO, accession number GSE148442.

## RESULTS

### NF-κB and IRAK4 activation correlate with T cell dysfunction

From TCGA database we observed strong positive correlation between MsigDB Biocarta NF-κB (M15285, contains 21 genes[13]) and "activated stroma" signature, defined by Moffitt et al to be associated with poor prognosis[14] (Fig, 1A, 1B). Gene expression signatures representing T cell and CAF status were described by Tirosh et al[15] and Spranger et al[16]. Using these signatures, we found that PDAC samples with high NF-κb scores exhibit markedly higher T cell exhaustion signatures (Fig. 1C, 1D). Overexpression or nuclear

translocation of the NF-κB family member, RELA, is the most widely used marker to represent NF-κB activation in PDAC samples[17]. High *RELA* expression is associated with poor progression-free survival (Log-rank $P = .02$) and a trend towards poor overall survival in PDAC (Log-rank $P = .072$, Suppl. Fig. 1A and 1B). *RELA* expression mild-positively correlates with the activated stroma signature (Fig. 1E), and negatively correlates with normal stroma signature (Fig. 1F). High *RELA* tumors also exhibit higher T cell exhaustion signature and lower pro-T cell cancer-associated fibroblast (CAF) signatures. (Fig. 1G, 1H). Expression of *RELA* mild-inversely correlate with T cell and cytotoxic T cell signatures (Suppl. Fig. 1C–E). These initial correlative observations prompted us to investigate whether targeting the NF-κB pathway or its upstream event can reverse T cell dysfunction in PDAC.

To establish the causality between tumor NF-κB and T cell response, we focus on IRAK4 kinase, which is constitutively activated and drives both the NF-κb and MAPK pathways in PDAC[6, 8]. We knocked out (KO) *IRAK4* using four lentiviruses encoding Cas9 and different single guided RNAs (sgIRAK4) in KP2, a cell line derived from the PDAC of a *p48*-Cre; $Tp53^{flox/WT}$; LSL-$KRAS^{G12D}$ mouse[11]. To exclude off-target effects, we re-expressed murine *IRAK4* cDNA in *IRAK4*-KO cells (Fig. 1I). By Gene Set Enrichment Analysis (GSEA), NF-κb and inflammatory response signatures were significantly downregulated in *IRAK4*-KO and restored in *IRAK4*-rescued cells (Fig. 1J). Interestingly, epithelial-mesenchymal transition (EMT) and Wnt/β-catenin signatures, which drives immune evasion in melanoma[16], were also downregulated following *IRAK4* ablation. Compared to *IRAK4*-KO cells, wild-type and *IRAK4*-rescued cells displayed a more “basal-like” tumor epithelial subtype which is independently associated with poor prognosis in PDAC[14] (Suppl. Fig. 1F) and congruent with our previous report showing activated IRAK4 to be poor prognostic[6]. The top Gene Ontology (GO) signatures downregulated in *IRAK4*-KO cells broadly fell into four categories: tumor-stromal reaction, MAPK pathway, inflammation, and migration/EMT, Fig. 1K). These data suggest that tumor IRAK4 may contribute to T cell dysfunction. To this end, we investigated the correlation of phosphorylated (p−) IRAK4 immunohistochemical (IHC, by H-score, Suppl. Fig. 1G) staining with the abundance of intratumoral $CD8^+$ T cells (by immunofluorescence) in a PDAC tissue microarray (TMA). In this TMA, tumor p-IRAK4 H-score mild-inversely correlated with $CD8^+$ T cell abundance (Fig. 1L).

## IRAK4 controls expression of chemokines and checkpoint ligands that suppress T cells

Further analysis of TCGA database showed that *IRAK4* expression positively correlates with T cell exhaustion in PDAC (Fig. 2A, 2B). In support, RNAseq data of *IRAK4*-KO KP2 cells showed several known immunosuppressive cytokines and chemokines to be significantly decreased (Fig. 2C), which we confirmed in independently-created control, *IRAK4*-KO and *IRAK4*-KO-rescued KP2 cells (Suppl. Fig. 2A) and using pharmacologic inhibition with CA-4948, a potent IRAK4 inhibitor (IRAK4i) (Suppl. Fig. 2B). Notably, checkpoint molecules including PD-L1 (encoded by *CD274*), Nectin2 and TIGIT were also downregulated following knockout or inhibition. We confirmed the suppression of PD-L1 protein by western blots using two different IRAK4i CA-4948 and AS2444697 (Fig. 2D), and also flow cytometry in *IRAK4*-ablated KP2 cells (Suppl. Fig. 2C). As parallel support, *IRAK4* expression positively correlates with *CCL2, IL33, CD274 and TIGIT* in TCGA database (Suppl. Fig. 2D). In addition to PD1, TIGIT is another T cell checkpoint

receptor that binds PVR (or CD155) and Nectin2 (or CD112) to promote immune evasion in PDAC[18] . Therefore, tumor IRAK4 may engage PD1 and TIGIT to impair T cells.

To discern the impact of tumor IRAK4 on $CD8^+$ T cell activity, we utilized the Nur77-GFP reporter mice, whose T cells express green fluorescence protein (GFP) by activation of T cell receptor, but not inflammatory stimuli[19]. We inoculated syngeneic wild-type (WT) or *IRAK4*-KO KP2 cells subcutaneously in Nur77-GFP mice and harvested the tumors 14 days later. *IRAK4*-KO KP2 tumors were significantly smaller (Fig. 2E). Remarkably, by immunofluorescence (IF) only ~15% of $CD8^+$ T cells infiltrating WT KP2 tumors expressed GFP, suggesting that the vast majority of intratumoral $CD8^+$ T cells were actually inactive or exhausted (Fig. 2F). Analysis of TCGA database showed extremely strong, positive correlation of T cell exhaustion and cytotoxic T cell signatures (Pearson r~0.9, Suppl. Fig. 2E–G), also suggesting that most infiltrative $CD8^+$ T cells are exhausted in PDAC. In comparison, significantly more $CD8^+$ T cells infiltrating *IRAK4*-KO tumors were activated, as demonstrated by GFP expression (Fig. 2F).

We next resorted to the KI ($KRAS^{G12D}$; $INK4A^{fl/fl}$) cell line, which forms tumors reproducibly and safely in the pancreas, the physiologically-relevant TME. Instead of genetic ablation, we utilized pharmacological approach. We found that treatment with CA-4948, resulted in smaller tumors (Fig. 2G) with lower Nectin2 and PD-L1 expression (Fig. 2H, 2I). Flow cytometry showed CA-4948-treated tumors were infiltrated with significantly more $CD8^+$ T cells, $CD4^+Foxp3^-CD44^{high}$($CD4^+$ T effector) cells and $CD8^+$ $CD44^{high}$ ($CD8^+$ T effector) cells (Fig. 2J, 2K), resulting in a higher $CD4^+$ Teffector/Treg ratio. Concomitant unbiased RNAseq analysis from the same tumors showed CA-4948-treated tumors to be significantly enriched for effector or activated $CD8^+$ T cell signatures (Fig. 2L), as well as downregulation of NF-κB, JAK-STAT and TLR cascades, RAS/MAPK, and EMT-related Hippo, Wnt and Notch signaling pathways (Suppl. Fig. 2H), demonstrating on-target effect. Overall, these data provide the experimental evidence that IRAK4 suppression can revitalize intratumoral T cells.

## Pharmacologic IRAK4 inhibition leads to inflammatory and T cell supportive TME

To obtain a deeper and unbiased understanding on how IRAK4 inhibition impacts CAFs and immune cell phenotypes we performed single cell RNA sequencing (scRNAseq) on isolated CAFs and infiltrating $CD45^+$ leukocytes from the PDAC of KPC mice treated with vehicle or CA-4948 starting from 6 weeks of age for totally 14 days. First, unsupervised clustering revealed different CAF subsets including myofibroblast-like (myCAFs), inflammatory CAFs (CAFs) antigen-resenting CAFs (apCAFs) and proliferating CAFs (Fig. 3A, Suppl. Fig 3A). We found that CA-4948 treatment resulted in decreased myCAF but increased iCAF population (Fig. 3B). To assess phenotypic changes in each CAF subsets we performed differential gene analysis (DEG) and GSEA using MsigDB Hallmark signatures. We observed a shift of all subsets towards an inflammatory phenotype, as discerned by increased TNF signaling, inflammatory response and angiogenesis signatures (Fig. 3C). In support, expression of *Il6* and *CXCL1* inflammatory cytokines were markedly enhanced in all subsets (Fig. 3D). Surprisingly there were many conserved changes in individual genes and GSEA pathways across multiple myeloid cell subsets Unsupervised clustering generated

all major leukocyte clusters (Fig. 3A). For innate immune cells, we identified three subsets of dendritic cells (cDC1, cDC2 and migratory DC), monocytes, tumor-associated macrophages and neutrophils with known and expected identity genes (Fig. 3E, Suppl. Fig 3B). We observed enrichment of allograft rejection signature in TAMs and monocytes, as well as coagulation, complement and oxidative phosphorylation signatures in neutrophils, monocytes and migratory DCs (Fig. 3G), also suggestive of acute inflammatory responses. In support, we observed a significant upregulation of multiple inflammatory cytokines (CCL2, 3,4 and 7, and CXCL1 and 2) across many of the myeloid subsets (Fig. 3H). While classical $T_H1$ recruiting chemokines CXCL9, 10 were not upregulated in myeloid cells, several of these upregulated chemokines are capable of recruiting T cells through CCR1, 2 and 3. Intriguingly, CA-4948 treatment did not seem to alter the proportion of M1- or M2 phenotypes of TAMs (Suppl. Fig. 3C–E). For adaptive immune cells, CA-4948 did not seem to greatly alter the composition of each subsets including B cells, plasma cells, CD4 T cells, CD4 Treg and CD8 T cells (Fig. 3I, 3J, Suppl. Fig. 3F). However, GSEA showed CA-4948 treatment resulted in markedly enhanced inflammatory signatures in $CD4^+$ and $CD8^+$ T cells (Fig. 3K, 3L), which is again supported by enhanced expression of inflammatory chemokines CCL2, 3,4 and 7, and CXCL1 and 2 (Fig. 3M). To independently confirm these findings, we treated a separate cohort of 6-week-old KPC mice with identical condition and performed multiple analyses (Fig. 3N). Consistent with previous findings in orthotopic KI models and scRNAseq, CA-4948 treatment resulted in decreased abundance of α-SMA (myCAF marker), in addition to Ly6G (marker for myeloid-derived suppressive cell, MDSC), Nectin2 and PD-L1 checkpoint ligands (Fig. 3O, 3P, 3Q, 3R). Flow cytometry showed no change in abundance of $CD4^+$ T cells, $CD4^+$ Treg, $CD8^+$ T subsets, granulocytes, monocytes and TAM, but significant increase of both $CD44^{high}$ $CD4^+$ and $CD44^{high}$ $CD8^+$ effector T cells (Fig. 3S, Suppl. Fig 3G). These data showed that CA-4948 qualitatively reprograms CAFs, innate and adaptive immune compartments towards an inflammatory phenotype which may favor tumor rejection.

## IRAK4 enhances *HAS2* expression and stromal hyaluronan to impair T cell response

Our RNAseq data from PDAC cell lines showed that IRAK4 suppression also downregulates signatures in connective tissue development, cell-substrate interaction and glycosaminoglycan biosynthesis (Fig. 1K, Supple. Fig. 2H). Indeed, PDAC of KPC mice treated with AS2444697 or CA-4948 displayed not only retarded neoplastic progression, but also lower Sirius red, Alcian blue and hyaluronan abundance (Fig. 4A–D). By applying a more stringent filter (changes >2-fold, false discovery rate FDR<0.5), we identified *Hyaluronan synthase 2* (*HAS2*), one of the three genes (*HAS1–3*) that governs hyaluronan (HA) synthesis[20], as one of the ten genes that are significantly affected by *IRAK4* expression (Fig. 4E). As support, TCGA database showed that *HAS2* positively correlates with *IRAK4* expression in PDAC samples (Fig. 4F). HAS2 protein expression was robustly detected in the epithelial compartment of pancreatic intraepithelial neoplasia (PanIN) lesions, PDAC and CAFs (Fig. 4G **left,** Suppl. Fig, 4A). Treatment with CA-4948 markedly reduced HAS2 expression in both PDAC cells and CAFs in KPC mice, as well in cultured PDAC cells (Fig. 4G **right,** Suppl. Fig. 4B). Specifically, expression of *HAS2*, but not *HAS1* or *HAS3*, is controlled by *IRAK4* in KP2 cells (Suppl. Fig 4C). Because the promoter region of *HAS2* gene contains multiple RELA/NF-κb binding sites[21], we hypothesize that IRAK4

controls *HAS2* transcription through activating RELA. Indeed, ablation of *IRAK4* abrogated RELA nuclear translocation (Supple. Fig. 4D), resulting in loss of RELA occupancy at the *HAS2* promoter regions as shown by ChIP-PCR assay (Suppl. Fig 4E). These results show that IRAK4 drives transcription of *HAS2* through nuclear translocation of RELA.

CAFs have often been regarded as the major producer of hyaluronan[22], but the regulatory mechanism has not been clearly described. Robust HAS2 protein expression was observed in three of four isolated PDAC CAF lines, compared to normal pancreatic fibroblasts SC00A5 (Suppl. 4F). Expression of HAS2 in SC00A5 and PDAC CAFs (CAF-2) could be reversibly induced by exposure to PDAC conditioned media (CM) (Suppl. Fig. 4G, 4H), suggesting presence of humoral factors in PDAC CM that drive *HAS2* expression in CAFs. Furthermore, CM from *IRAK4*-silenced PDAC cells was unable to induce *HAS2* expression in CAFs (Suppl. Fig. 4I), suggesting that tumor IRAK4 controls humoral factors that induce *HAS2* in CAFs. Notably, PDAC CM was able to induce hyaluronan production in CAFs, but not when CAFs were co-treated with CA-4948, suggesting IRAK4 is required for *HAS2* expression and hyaluronan production in CAFs (Suppl. Fig. 4J). As confirmation, injection of KP2 cells into global *IRAK4*-null mice resulted in tumors with significantly reduced hyaluronan content (Suppl. Fig. 4K). These results showed that IRAK4 controls *HAS2* expression in both PDAC cells and CAFs, and that *HAS2* expression in CAFs is additionally regulated by PDAC cells.

Analysis of TCGA database showed that high *HAS2* expression is associated with inferior overall survival in PDAC (Fig. 4H). Interestingly, *HAS2* expression also correlates positively with T cell exhaustion (Fig. 4I, Suppl. Fig. 4L), leading us to hypothesize that IRAK4-induced T cell dysfunction could also be partly mediated through *HAS2* expression. Indeed, while *IRAK4*-KO tumors were smaller and had increased intratumoral $CD8^+$ T cell infiltration compared to vector controls, these changes were reversed by ectopic re-expression of *HAS2 in IRAK4*-KO cells (Fig. 4J, 4K). Suppressive factors mediated by *IRAK4*, including PD-L1, were also downregulated in KP2 and Capan-1 cells treated with a HAS2 inhibitor 4-Methylumbelliferone[23] (4-MU, Fig. 4L, Suppl. Fig. 4M). In support, analysis of TCGA databased showed positive correlation between the expression of *HAS2* with *CD274 and TIGIT* (Suppl. Fig. 4N), indicating that HAS2 may independently drive T cell dysfunction. To show this, we overexpressed murine *HAS2* in KP2 cells and inoculated them in syngeneic C57BL/6J mice. Compared to control tumors, *HAS2*-overexpressing tumors were larger, had higher intratumoral hyaluronan content, decreased intratumoral $CD8^+$ T cells, and notably decreased granulocytes, increased monocytes, granulocyte-MDSC and total TAMs (Fig. 4M, 4N, 4O). These data showed that tumor IRAK4 drives immunosuppressive TME and T cell dysfunction in part through mediating intratumoral HAS2 expression.

## Conditional deletion of tumor *IRAK4* produces PDAC with increased T cell infiltration

To clearly establish the role of tumor IRAK4, we generated conditional *IRAK4*-deleted *p48-Cre/TP53*$^{fl/f}$*/LSL-KRAS*$^{G12D}$ mice (*IRAK4*$^{fl/f}$ KPC), in which exons 2–12 of the *IRAK4* gene was flanked by loxP sequence and excised in a *p48*-Cre dependent manner. We confirmed loss of IRAK4 IHC staining in the PDAC epithelium but not in stromal or

immune cells in *IRAK4*$^{fl/f}$ KPC mice (Fig. 5A). Although there was no difference in the natural survival between WT and *IRAK4*$^{fl/f}$ KPC mice (Suppl. Fig. 5A), serial histologic comparison of age-matched pancreata of WT and *IRAK4*$^{fl/f}$ KPC mice showed a retardation of histologic progression, culminating in significantly less PDAC burden, relatively more PanIN and necrotic areas and tumors that were ~50% the size of WT KPC mice (Fig. 5B, 5C, 5D), resonating the effect of CA-4948 (Fig. 4A). None of the *IRAK4*$^{fl/f}$ KPC mice developed ascites at euthanasia (Suppl. Fig. 5B). Compared to WT mice, *IRAK4*$^{fl/f}$ pancreata had higher retention of amylase expression and lower abundance of Sirius red staining (Fig. 5E, Suppl. Fig. 5C). However, end-staged *IRAK4*$^{fl/f}$ KPC pancreata retained around ~8% of amylase$^{+}$ area, which could explain their demise. Consistent with our finding that tumor IRAK4 controls *HAS2* expression in PDAC and CAFs, *IRAK4*$^{fl/f}$ pancreata showed markedly lower HAS2 IHC staining in both PDAC cells and CAFs (Fig. 5F) and correspondingly reduced Alcian blue staining (Fig. 5G).

Further IF staining showed that *IRAK4*$^{fl/f}$ PDAC tumors had significantly lower pan-cytokeratin (Pan-CK) staining, consistent with lower PDAC burden, but significantly higher abundance of intratumoral CD45$^{+}$ leukocytes, CD4$^{+}$ and CD8$^{+}$ T cells (Fig. 5H, 5I), which were also more proliferative by Ki-67 staining (Fig. 5J). Phenotypically, higher percentage of circulating CD8$^{+}$ T cells isolated from the blood of *IRAK4*$^{fl/f}$ KPC mice expressed TNF, IFN$\gamma$ and IL-2 (Fig. 5K). Compared to WT tumors, higher percentage of CD8$^{+}$T cells isolated from autochthonous *IRAK4*$^{fl/f}$ KPC tumors expressed TNF or higher level of IL-2, as well as lower level of exhaustion marker PD1 and LAG3 (Fig. 5L), resonating upregulated TNF signaling CD4$^{+}$ and CD8$^{+}$ T cells from scRNAseq analysis in KPC tumors (Fig. 3K, 3L). Functionally, CD8$^{+}$ T cells isolated from *IRAK4*$^{fl/f}$ PDAC were also more proliferative in vitro (Suppl. Fig. 5D). Together, these data showed that loss of tumor *IRAK4* resulted in increased activity of tumor-infiltrative and peripheral CD8$^{+}$ T cells.

## Conditional *IRAK4*-deleted KPC mice respond to checkpoint immunotherapy

The increased abundance and activity of T cells in *IRAK4*$^{fl/f}$ KPC mice prompted us to test whether these T cells could be unleashed for anti-tumor response. We treated 6-week-old WT or *IRAK4*$^{fl/f}$ KPC mice with checkpoint immunotherapy (anti-CTLA4 plus anti-PD1) biweekly for 5 doses. Low dose gemcitabine (25mg/kg) was included to induce tumor damage and potentially antigen release for T cell recognition. Strikingly, immunotherapy significantly prolonged the survival of *IRAK4*$^{fl/f}$ KPC mice, with two mice survived greater than 120 days after treatment completion, while it was completely ineffective in WT KPC mice (Fig. 6A). When euthanized, the pancreata of immunotherapy-treated *IRAK4*$^{fl/f}$ mice showed markedly reduced PDAC lesions and increased immune infiltration (Fig. 6B, blinded interpretation by GI pathologist MBR). As confirmation, IF showed markedly reduced pan-CK area and higher abundance of CD45$^{+}$ leukocytes, CD4$^{+}$ and CD8$^{+}$ T cells which were also more proliferative in immunotherapy-treated *IRAK4*$^{fl/f}$ compared to WT pancreata (Fig. 6C, 6D, 6E). To determine if the surviving PDAC cells from the terminal *IRAK4*$^{fl/f}$ KPC mice were still responsive to immunotherapy, we isolated two KPC cell lines each from terminal WT and *IRAK4*$^{fl/f}$ KPC mice. Loss of IRAK4 expression in *IRAK4*$^{fl/f}$ KPC cell lines were confirmed by western blots prior to subcutaneous injection into regular C57BL/6J mice (Suppl. Fig. 6B). One week after inoculation, all mice were treated

with immunotherapy. Again, *IRAK4*$^{fl/f}$ KPC tumors remained sensitive to immunotherapy, whereas wild-type tumors were completely refractory (Fig. 6F).

Because both tumor and stromal IRAK4 have pro-tumorigenic role in PDAC, we attempted to generate global *IRAK4*-knockout KPC mice, but with no success. Interestingly, global heterozygous *IRAK4*$^{+/-}$ KPC mice gave rise to PDAC tumors that had relatively lower hyaluronan and Sirius Red staining (Fig. 6G). Remarkably, *IRAK4*$^{+/-}$ KPC mice survived significantly longer than wild-type littermates from birth (median survival 79 vs. 62 days, $p<0.001$) and responded to immunotherapy, which significantly extended their survival (Fig. 6H).

## Preclinical efficacy of IRAK4 inhibitor-based therapeutic strategies in PDAC

We next tested the therapeutic efficacy of pharmacologic IRAK4 inhibitors separately with chemotherapy and immunotherapy. First, we treated 6-week-old WT autochthonous KPC mice with vehicle, CA-4948 or chemotherapy (gemcitabine plus paclitaxel) alone or in combination until humane endpoints. While CA-4948 alone prolonged the survival of KPC mice, the combination of CA-4948 plus chemotherapy more than doubled the survival of KPC mice compared to vehicle or chemotherapy alone (Fig. 7A). When euthanized, the pancreata of combo-treated mice were significantly smaller (Fig. 7B) and displayed higher degree of apoptosis by cleaved caspase-3 staining and marked disruption of Pan-CK architecture (Fig. 7C).

Next, we tested whether IRAK4 inhibition would render immunotherapy effective. Intriguingly, CA-4948 potentiated anti-CTLA4, but had no effect when combined with anti-PD1, potentially because CA-4948 alone is sufficient to downregulate PD-L1 as our data had shown. However, the combination of CA-4948 with dual anti-CTLA and anti-PD1 achieved the most profound anti-tumor effect (Fig. 7D, 7E). As parallel confirmation, another IRAK4 inhibitor AS2444697 also synergized with immunotherapy in curbing KP2 tumor growth in syngeneic C57BL/6J model (Suppl. Fig. 7A, 7B). The anti-tumor effect of CA-4948 plus dual immunotherapy was completely abrogated when either $CD4^+$ or $CD8^+$ T cells were depleted with neutralizing antibodies (Fig. 7F, 7G, Suppl. Fig. 7A–D), demonstrating the requirement for both $CD4^+$ and $CD8^+$ T cells in tumor rejection. We next tested this strategy in autochthonous KPC mice. While AS2444697 or CA-4948 alone was able to mildly prolong the survival of KPC mice, the combination of either IRAK4i with checkpoint immunotherapy significantly extended survival (Fig. 7H). Combo-treated end-stage KPC mice had significantly smaller tumor burden in their pancreata (Fig. 7I), and only one of 33 combo-treated mice had ascites when sacrificed (Fig. 7J). Strikingly, combo-treated pancreata showed very little residual PDAC areas, and instead were occupied by PanINs, inflammatory and necrotic areas (Fig. 7K). Several combo-treated tumors contained tertiary lymphoid structures (middle panel), a histologic feature strongly associated with productive anti-tumor immunity[24]. As expected, combo-treated tumors were heavily infiltrated with $CD4^+$ and $CD8^+$ T cells (Fig. 7L), resonating findings in *IRAK4*$^{fl/f}$ KPC mice.

## DISCUSSION

Suppressive CAFs, myeloid cells and chemokines are barriers that drive T cell dysfunction in PDAC[25]. The strong positive correlation between cytotoxic T cell and T cell exhaustion signatures that we observed in PDAC samples, also seen in melanoma[15], suggests that removal of exhaustion programs is critical in unleashing T cell response. We now provide multiple lines of evidence that targeting IRAK4 overcomes these barriers. We show that tumor IRAK4 controls production of several immunosuppressive chemokines, cytokines and checkpoint ligands including PD-L1 and Nectin2. Suppression of IRAK4 by genetic ablation or pharmacologic inhibition resulted in infiltration of T cells that are more activated and readily unleashed by checkpoint inhibitors. Mechanistically, T cell exhaustion markers such as PD1 are driven by upregulation of transcriptional factors NFAT and BATF[26, 27], but the signaling pathways that upregulate these factors remain unclear. Chronic engagement of TLR7 or chronic infection with HIV leads to anergy of $CD4^+$ T cells via NFATc2[28]. Therefore, we posit that sustained IL-1R/TLR engagement may signal through IRAK4 to upregulate the transcription factors that ultimately exhaust anti-tumor T cells.

Our data show that a mechanism by which tumor IRAK4 drives T cell exhaustion is NF-κB-dependent upregulation of *HAS2*, a key enzyme that synthesizes hyaluronan. PDAC tumors are characterized by high hyaluronan content, which raises interstitial pressure and collapses tumor vasculature essential for delivery of chemotherapeutics[29]. Unfortunately, addition of hyaluronidase to chemotherapy did not improve patient survival in clinical trials[30]. However, these setbacks should instead prompt more in-depth studies to develop alternative therapeutic strategies against hyaluronan. Apart from being a structural proteoglycan, hyaluronan binds surface CD44 receptor to promote stem-like phenotypes including invasion, metastasis and cellular survival[31]. We found that HAS2 inhibitor lower the expression of suppressive cytokines and chemokines that overlap with IRAK4, and overexpression of HAS2 alone in PDAC cells markedly reduced $CD8^+$ T cell infiltration. These results are congruent with a recent report that targeting tumor-intrinsic hexosamine biosynthesis sensitizes pancreatic cancer to anti-PD1 therapy, in part by abrogating hyaluronan synthesis[32]. In light of multiple recent studies showing that type 1 collagen is tumor-restrictive, at least in part by augmenting immune suppression[33, 34], targeting hyaluronan as an immunotherapeutic strategy should be vigorously investigated.

An important finding from our single cell RNAseq analysis demonstrates that IRAK4 inhibition resulted in myeloid and CAF reprograming towards acute inflammatory responses, which may reflect successful conversion of PDAC from an immunologically “cold” tumor into a “hot“ tumor. The intrinsic role of IRAK4 in T cells remains controversial. Using almost identical *in vitro* and *in vivo* stimulation assays but independently generated *IRAK4-null* C57BL/6 mice, Suzuki et al showed that *IRAK4-null* mice are defective in T-cell activation[35], whereas Kawagoe et al showed that *IRAK4-null* T cells are indistinguishable from wild-type T cells[36]. Here we show that systemic pharmacologic IRAK4 inhibition actually revitalizes intratumoral T cells, and heterozygous global $IRAK4^{+/-}$ KPC mice were responsive to immunotherapy, mitigating the concerns that systemic IRAK4 inhibition may blunt T cell response. CA-4948 is the only IRAK4 inhibitor that has entered clinical trial for patients with relapsed/refractory hematopoietic

malignancies (NCT03328078). Therefore, our study provides an immediately translatable therapeutic strategy that can be advanced into the clinic for PDAC patients.

## Supplementary Material

Refer to Web version on PubMed Central for supplementary material.

## Funding support:

NIH R37CA219697-01, NIH 1P50CA196510-01A1, American Cancer Society (RSG-17-203-01-TBG), Alvin J. Siteman Cancer Center Siteman Investment Program (supported by Barnard Trust and The Foundation for Barnes-Jewish Hospital).

Study concept and design: KHL, VS, DZ; acquisition, analysis and interpretation of data: VK, DZ, PBD, VEL, XL, LK, HPC, LL, PMG, MBR, DGD, KHL; drafting of the manuscript: VK, DGD, KHL ; critical revision of the manuscript for important intellectual content: DGD, KHL; statistical analysis: PBD, VEL, DGD, KHL; obtained funding: KHL; technical support: BLK, LL; study supervision: KHL

All data, analytic methods, and study materials will be made available to other researchers upon request.

## REFERENCES

Author names in bold designate shared co-first authorship

1. Wattenberg MM, Beatty GL. Overcoming immunotherapeutic resistance by targeting the cancer inflammation cycle. Semin Cancer Biol 2020.
2. Ochi A, Graffeo CS, Zambirinis CP, et al. Toll-like receptor 7 regulates pancreatic carcinogenesis in mice and humans. J Clin Invest 2012;122:4118–29. [PubMed: 23023703]
3. Zambirinis CP, Levie E, Nguy S, et al. TLR9 ligation in pancreatic stellate cells promotes tumorigenesis. J Exp Med 2015;212:2077–94. [PubMed: 26481685]
4. Ling J, Kang Y, Zhao R, et al. KrasG12D-induced IKK2/beta/NF-kappaB activation by IL-1alpha and p62 feedforward loops is required for development of pancreatic ductal adenocarcinoma. Cancer Cell 2012;21:105–20. [PubMed: 22264792]
5. Dunne A, O'Neill LA. The interleukin-1 receptor/Toll-like receptor superfamily: signal transduction during inflammation and host defense. Sci STKE 2003;2003:re3.
6. Zhang D, Li L, Jiang H, et al. Constitutive IRAK4 Activation Underlies Poor Prognosis and Chemoresistance in Pancreatic Ductal Adenocarcinoma. Clin Cancer Res 2017;23:1748–1759. [PubMed: 27702822]
7. Dodhiawala PB, Khurana N, Zhang D, et al. TPL2 enforces RAS-induced inflammatory signaling and is activated by point mutations. J Clin Invest 2020.
8. Zhang D, Li L, Jiang H, et al. Tumor-Stroma IL1beta-IRAK4 Feedforward Circuitry Drives Tumor Fibrosis, Chemoresistance, and Poor Prognosis in Pancreatic Cancer. Cancer Res 2018;78:1700–1712. [PubMed: 29363544]
9. Garg B, Giri B, Modi S, et al. NFkappaB in Pancreatic Stellate Cells Reduces Infiltration of Tumors by Cytotoxic T Cells and Killing of Cancer Cells, via Up-regulation of CXCL12. Gastroenterology 2018;155:880–891 e8. [PubMed: 29909021]
10. Suzuki N, Suzuki S, Duncan GS, et al. Severe impairment of interleukin-1 and Toll-like receptor signalling in mice lacking IRAK-4. Nature 2002;416:750–6. [PubMed: 11923871]
11. Jiang H, Hegde S, Knolhoff BL, et al. Targeting focal adhesion kinase renders pancreatic cancers responsive to checkpoint immunotherapy. Nat Med 2016;22:851–60. [PubMed: 27376576]
12. Lim KH, Langley E, Gao F, et al. A clinically feasible multiplex proteomic immunoassay as a novel functional diagnostic for pancreatic ductal adenocarcinoma. Oncotarget 2017;8:24250–24261. [PubMed: 28445954]
13. Liberzon A, Birger C, Thorvaldsdottir H, et al. The Molecular Signatures Database (MSigDB) hallmark gene set collection. Cell Syst 2015;1:417–425. [PubMed: 26771021]

14. Moffitt RA, Marayati R, Flate EL, et al. Virtual microdissection identifies distinct tumor- and stroma-specific subtypes of pancreatic ductal adenocarcinoma. Nat Genet 2015;47:1168–78. [PubMed: 26343385]
15. Tirosh I, Izar B, Prakadan SM, et al. Dissecting the multicellular ecosystem of metastatic melanoma by single-cell RNA-seq. Science 2016;352:189–96. [PubMed: 27124452]
16. Spranger S, Bao R, Gajewski TF. Melanoma-intrinsic beta-catenin signalling prevents anti-tumour immunity. Nature 2015;523:231–5. [PubMed: 25970248]
17. Wang W, Abbruzzese JL, Evans DB, et al. The nuclear factor-kappa B RelA transcription factor is constitutively activated in human pancreatic adenocarcinoma cells. Clin Cancer Res 1999;5:119–27. [PubMed: 9918209]
18. Freed-Pastor WA, Lambert LJ, Ely ZA, et al. The CD155/TIGIT axis promotes and maintains immune evasion in neoantigen-expressing pancreatic cancer. Cancer Cell 2021;39:1342–1360 e14. [PubMed: 34358448]
19. Moran AE, Holzapfel KL, Xing Y, et al. T cell receptor signal strength in Treg and iNKT cell development demonstrated by a novel fluorescent reporter mouse. J Exp Med 2011;208:1279–89. [PubMed: 21606508]
20. Toole BP. Hyaluronan: from extracellular glue to pericellular cue. Nat Rev Cancer 2004;4:528–39. [PubMed: 15229478]
21. Saavalainen K, Tammi MI, Bowen T, et al. Integration of the activation of the human hyaluronan synthase 2 gene promoter by common cofactors of the transcription factors retinoic acid receptor and nuclear factor kappaB. J Biol Chem 2007;282:11530–9. [PubMed: 17307735]
22. Hosein AN, Brekken RA, Maitra A. Pancreatic cancer stroma: an update on therapeutic targeting strategies. Nat Rev Gastroenterol Hepatol 2020;17:487–505. [PubMed: 32393771]
23. Kultti A, Pasonen-Seppanen S, Jauhiainen M, et al. 4-Methylumbelliferone inhibits hyaluronan synthesis by depletion of cellular UDP-glucuronic acid and downregulation of hyaluronan synthase 2 and 3. Exp Cell Res 2009;315:1914–23. [PubMed: 19285976]
24. Sautes-Fridman C, Petitprez F, Calderaro J, et al. Tertiary lymphoid structures in the era of cancer immunotherapy. Nat Rev Cancer 2019;19:307–325. [PubMed: 31092904]
25. Ho WJ, Jaffee EM, Zheng L. The tumour microenvironment in pancreatic cancer - clinical challenges and opportunities. Nat Rev Clin Oncol 2020.
26. Agnellini P, Wolint P, Rehr M, et al. Impaired NFAT nuclear translocation results in split exhaustion of virus-specific CD8+ T cell functions during chronic viral infection. Proc Natl Acad Sci U S A 2007;104:4565–70. [PubMed: 17360564]
27. Martinez GJ, Pereira RM, Aijo T, et al. The transcription factor NFAT promotes exhaustion of activated CD8(+) T cells. Immunity 2015;42:265–278. [PubMed: 25680272]
28. Dominguez-Villar M, Gautron AS, de Marcken M, et al. TLR7 induces anergy in human CD4(+) T cells. Nat Immunol 2015;16:118–28. [PubMed: 25401424]
29. Jacobetz MA, Chan DS, Neesse A, et al. Hyaluronan impairs vascular function and drug delivery in a mouse model of pancreatic cancer. Gut 2013;62:112–20. [PubMed: 22466618]
30. Van Cutsem E, Tempero MA, Sigal D, et al. Randomized Phase III Trial of Pegvorhyaluronidase Alfa With Nab-Paclitaxel Plus Gemcitabine for Patients With Hyaluronan-High Metastatic Pancreatic Adenocarcinoma. J Clin Oncol 2020;38:3185–3194. [PubMed: 32706635]
31. Toole BP, Slomiany MG. Hyaluronan: A constitutive regulator of chemoresistance and malignancy in cancer cells. Seminars in Cancer Biology 2008;18:244–250. [PubMed: 18534864]
32. Sharma NS, Gupta VK, Garrido VT, et al. Targeting tumor-intrinsic hexosamine biosynthesis sensitizes pancreatic cancer to anti-PD1 therapy. J Clin Invest 2020;130:451–465. [PubMed: 31613799]
33. Bhattacharjee S, Hamberger F, Ravichandra A, et al. Tumor restriction by type I collagen opposes tumor-promoting effects of cancer-associated fibroblasts. J Clin Invest 2021;131.
34. Chen Y, Kim J, Yang S, et al. Type I collagen deletion in alphaSMA(+) myofibroblasts augments immune suppression and accelerates progression of pancreatic cancer. Cancer Cell 2021;39:548–565 e6. [PubMed: 33667385]
35. Suzuki N, Suzuki S, Millar DG, et al. A critical role for the innate immune signaling molecule IRAK-4 in T cell activation. Science 2006;311:1927–32. [PubMed: 16574867]

36. Kawagoe T, Sato S, Jung A, et al. Essential role of IRAK-4 protein and its kinase activity in Toll-like receptor-mediated immune responses but not in TCR signaling. J Exp Med 2007;204:1013–24. [PubMed: 17485511]

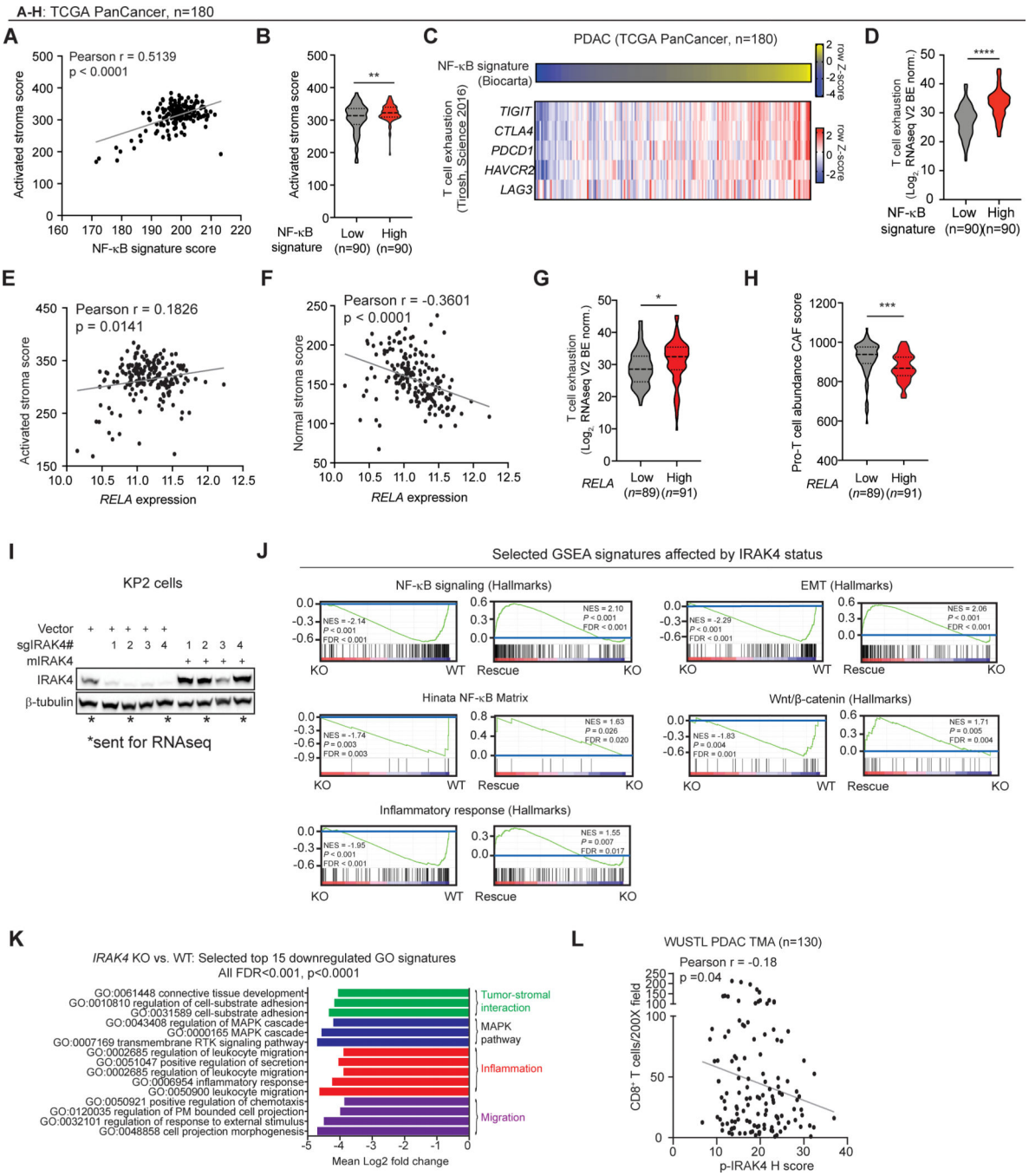


**Figure 1. NF-κB and IRAK4 activation correlate with T cell dysfunction.**

(*A*) Correlation scatter plot with Pearson coefficient (*r*) of activated stroma vs. NF-κB signature scores (Log2 RNAseqV2, BE norm.) in PDAC samples from TCGA. (*B*) Violin plot showing activated stroma scores in PDAC samples with high vs. low (by median) NF-κB scores. (*C*) Heatmaps depicting NF-κB signature score and expression of genes associated with T cell exhaustion across TCGA PDAC samples. (*D*) Violin plot showing T cell exhaustion scores in high vs. low NF-κB samples. Three outliers were removed for *RELA* expression by ROUT (*Q* = 5%). Gene sets lists are provided in Supplementary

Table 1. (*E, F*) Correlation scatter plots of activated and normal stroma signatures vs. *RELA* mRNA expression in PDAC samples from TCGA. (*G, H*) Violin plots showing T cell exhaustion or Pro-T cell abundance CAF signature scores in high vs. low (by median) *RELA* PDAC samples. (*I*) Western blots showing IRAK4 expression in CRISPR-mediated *IRAK4*-KO (sg*IRAK4*) and m*IRAK4*-rescued KP2 cells. (*J*) GSEA plots of selected gene signatures using "C6: Oncogenic Signatures" and "Hallmarks" gene-set databases in WT, *IRAK4*-KO and m*IRAK4*-rescue KP2 cells. (*K*) Bar graph depicting $Log_2$ fold change of various GO signatures in *IRAK4*-KO vs. control KP2 cells. (*L*) Correlation scatter plot of $CD8^+$ T abundance vs. p-IRAK4 H-score in a Wash U PDAC TMA consisting of 130 patients. (*$P < .05$, **$P < .01$, ***$P < .001$, ****$P < .0001$ by ANOVA or two-tailed unpaired t-test).

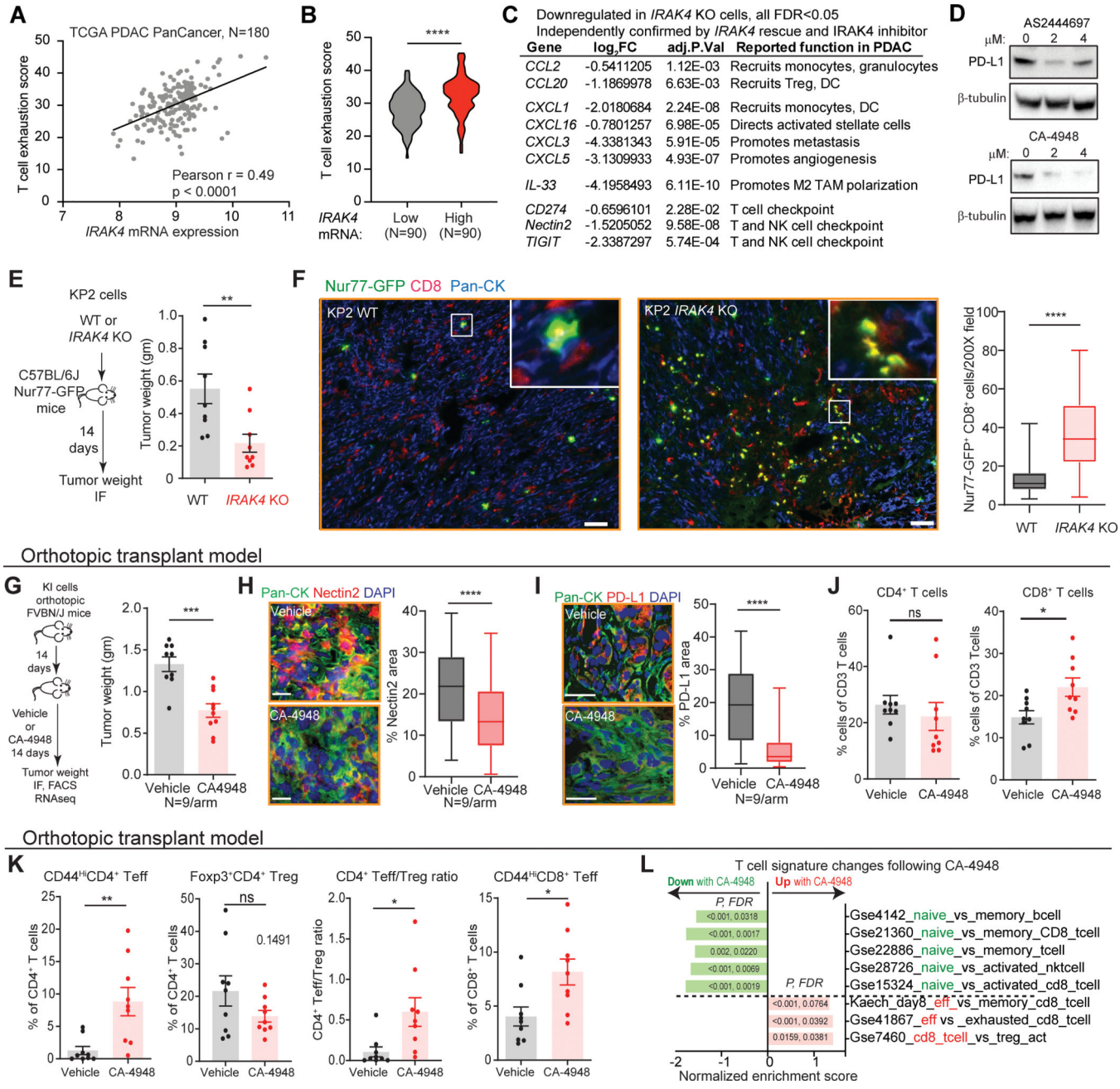


**Figure 2. IRAK4 controls expression of T cell suppressive factors.**

(*A, B*) Correlation and violin plots of T cell exhaustion score vs. *IRAK4* expression from PDAC TCGA data. (*C*) Primary RNAseq data showing changes in expression of the selected genes (FDR<0.05) in *IRAK4*-KO relative to control KP2 cells. (*D*) Western blots showing reduced PD-L1 expression in KP2 cells treated with two different IRAK4i for 24 hours. (*E*) Experimental schematics and weights of WT vs. *IRAK4*-KO KP2 tumors from Nur77-GFP reporter mice harvested 14 days after subcutaneous inoculation (N=9 mice/arm). (*F*) Representative co-IF images and quantification of dual-positive Nur77-GFP$^{+}$ (green) and CD8$^{+}$ (red) T cells in WT or *IRAK4*-KO tumors. (*G*) Schematics and weights

of tumors from FVB/NJ mice orthotopically inoculated with KI cells and treated with vehicle or CA-4948 (N=9 mice/arm). (*H, I*) Representative co-IF images and quantification of dual-positive Pan-CK and Nectin2 or PD-L1 areas in vehicle- or CA-4948-treated tumors. (*J, K*) FACS-based quantification of intratumoral $CD4^+$, $CD8^+$, $CD4^+$ effector ($CD4^+Foxp3^-CD44^{high}$), T regulatory cells ($CD4^+Foxp3^+$), $CD4^+$ Teff/Treg ratio, and $CD8^+$ effector ($CD8^+CD44^{high}$) in vehicle- or CA-4948-treated tumors. (*L*) Bar graph showing enrichment of selected immunologic gene signatures in vehicle- or CA-4948-treated KI tumors by RNAseq. “C7: Immunologic Signature” database was used from MSigDB. (*$P <$ .05, **$P <$ .01, ***$P <$ .001, ****$P <$ .0001 by ANOVA or two-tailed unpaired t-test; scale bars 50μM).

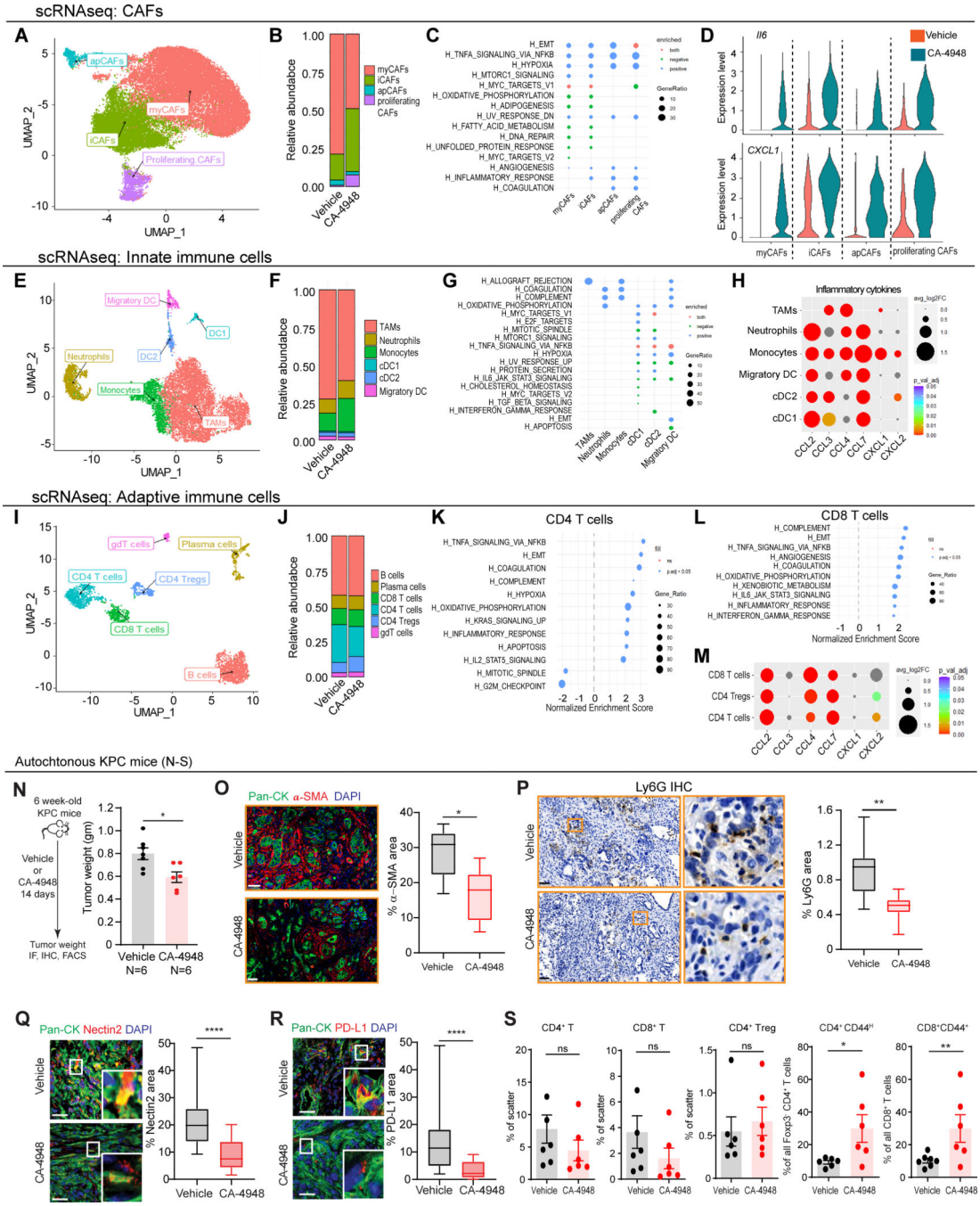


**Figure 3. Pharmacologic IRAK4 inhibition leads to inflammatory and T cell supportive TME.**

(*A*) UMAP plot, (*B*) relative abundance, (*C*) changes in selected MsigDB Hallmark signaling pathways and (*D*) expression of *IL6* and *CXCL1* of different subtypes of isolated CAFs from integrated vehicle- and CA-4948-treated KPC tumors (N=4 mice/arm). (*E*) UMAP plot, (*F*) relative abundance, (*G*) changes in selected MsigDB Hallmark signaling pathways and (*H*) DotPlot showing expression of the selected inflammatory chemokines of different myeloid populations (TAMs, DCs, neutrophils, and monocytes) in isolated CD45$^{+}$ leukocytes isolated from integrated vehicle-and CA-4948-treated KPC tumors. (*I*)

UMAP plot, (*J*) relative abundance, (*K, L*) changes in selected MsigDB Hallmark signaling pathways and (*M*) DotPlot showing expression of the selected inflammatory chemokines in different adaptive immune cell populations (B cells, plasma cells and different T subsets), isolated $CD45^+$ leukocytes from integrated vehicle-and CA-4948-treated KPC tumors. For all UMAP plots, colors represent clusters identified by Seurat clustering and/or by canonical gene expression. For al DotPlots, dot size represents average LogFC in CA-4948-treated tumors compared to vehicle-treated and colors represent adjusted *P* values. (*N*) Experimental schematics on autochthonous KPC mice treated as indicated and final tumor weights (N=6 mice/arm). Representative co-IF or IHC images and quantification of (*O*) α-SMA; (*P*) Ly6G; (*Q*) Nectin2; (*R*) PD-L1 abundance in vehicle- or CA-4948-treated KPC tumors (N=6/arm). (*S*) FACS-based quantification of the indicated intratumoral T cell subsets harvested from KPC mice in (N). (**P* < .05, ***P* < .01, ****P* < .001, *****P* < .0001 by ANOVA or two-tailed unpaired t-test; scale bars 50μM).

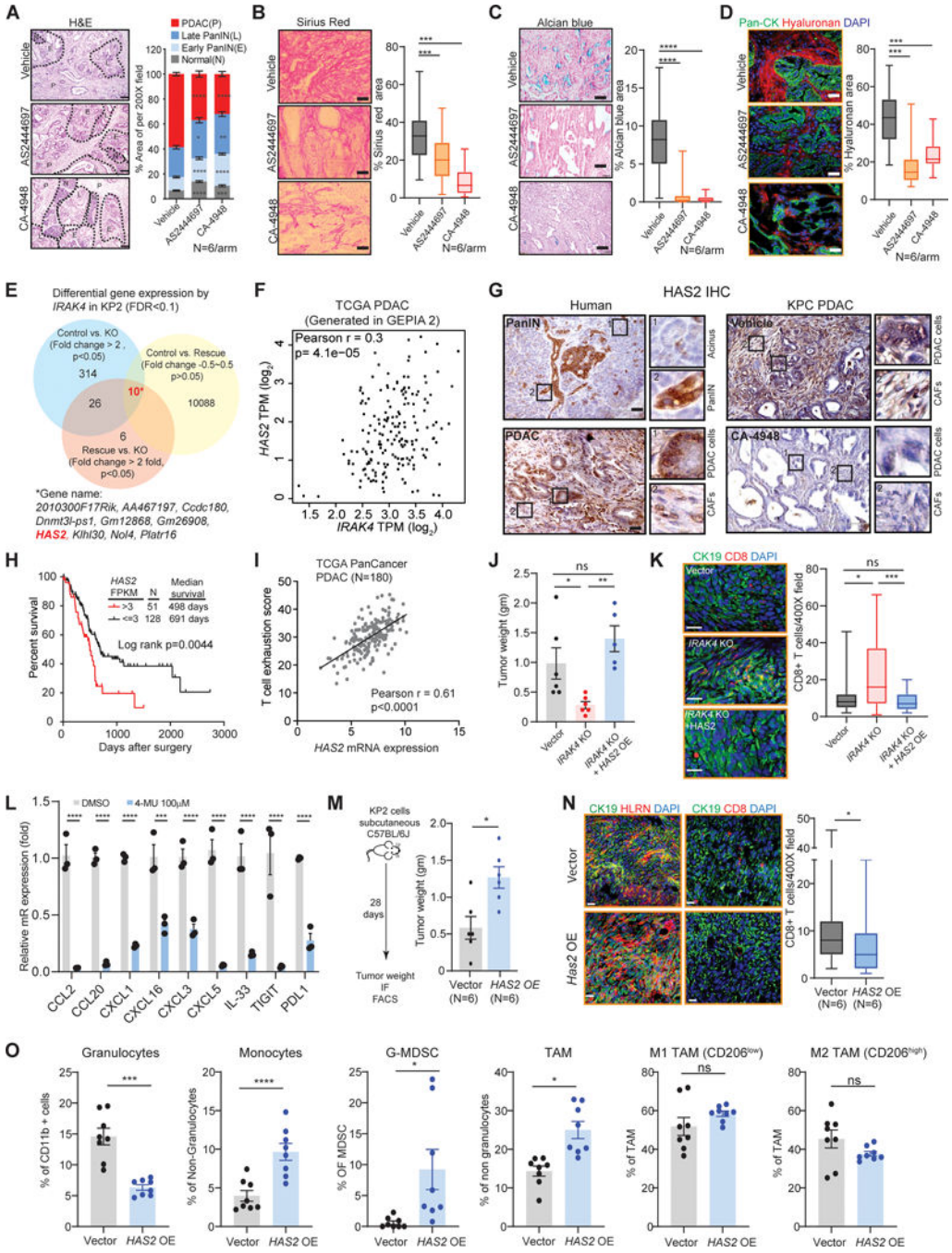


**Figure 4. IRAK4 enhances *HAS2* expression and stromal hyaluronan to impair T cell response.**

(*A-D*) Representative images and quantification of H&E histopathological features, Sirius red, Alcian blue and hyaluronan staining in the pancreata of KPC mice treated as indicated until humane endpoints. (*E*) Venn diagram of selected genes (>2-fold expression differences and FDR<0.1) in control vs. *IRAK4*-KO cells or *IRAK4*-KO-rescue vs. *IRAK4*-KO KP2 cells. Ten genes (*) fit the criteria and were listed. (*F*) Correlation plot of *HAS2* vs. *IRAK4* mRNA expression in TCGA PDAC database (generated from GEPIA 2). (*G*) Representative HAS2 IHC images in human PanIN and PDAC tissues, and in KPC tumors treated with

vehicle or CA-4948 for two weeks. (*H*) Kaplan-Meier survival of PDAC patients from TCGA stratified by *HAS2* mRNA expression using FPKM (fragments per kilobase of exon model per million reads mapped). (*I*) Correlation plot of *HAS2* mRNA expression vs. T-cell exhaustion score in TCGA PDAC samples. (*J*) Final weights of KP2 tumors expressing vector, an sg*IRAK4*, or sg*IRAK4* plus ectopic murine *HAS2* expression after 28 days from inoculation in C57BL/6J mice (N=6 mice/arm). (*K*) Representative co-IF images and quantification of $CD8^+$ T cells (red) in the indicated KP2 tumors. (*L*) Quantitative RT-PCR showing changes expression of the indicated genes in KP2 cells treated with DMSO or 4-MU 100μM for 72 hours. (*M*) Experimental schematic and (*N*) representative co-IF images and quantification of $CD8^+$T cells in control vs. *HAS2*-overexpressing KP2 tumors. (*O*) FACS-based quantification of the indicated myeloid subsets in control vs. *HAS2*-overexpressing KP2 tumors (N-8/arm) in a separate experiment. (**P* < .05, ***P* < .01, ****P* < .001, *****P* < .0001 by ANOVA or two-tailed unpaired t-test; scale bars 50μM).

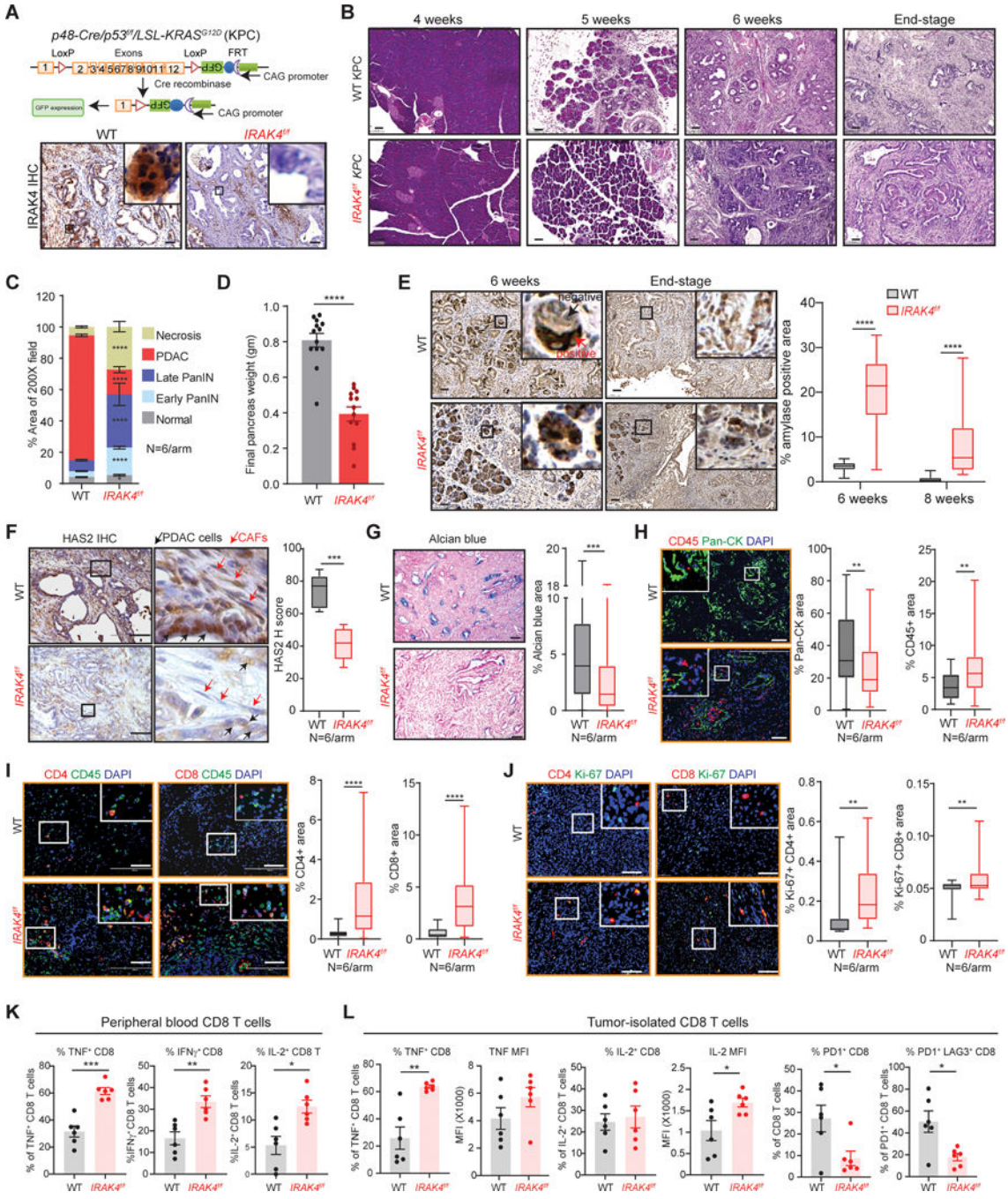


**Figure 5. Conditional deletion of tumor *IRAK4* produces PDAC with increased T cell infiltration.**

(*A*) Conditional knockout strategy of *IRAK4* gene in KPC mice and IHC picture confirming loss of tumor-intrinsic IRAK4 protein in *IRAK4*$^{fl/f}$ KPC mice. (*B*) Serial age-matched H&E images, (*C,D)* quantification of different histologic stages and final weights of end-staged pancreata of WT vs. *IRAK4*$^{fl/f}$ KPC mice (blinded analysis by GI pathologist). (*E*) Representative IHC images and quantification of amylase IHC in the pancreata of 6- and end-staged WT vs. *IRAK4*$^{fl/f}$ KPC mice. (*F*) Representative HAS2 IHC images and H-score measured using automated scanner and HALO software in the pancreata of end-staged WT

vs. *IRAK4*$^{fl/f}$ KPC mice. (*G-J*) Representative IHC and IF images and quantification of Alcian blue, Pan-CK, CD45, CD4 and CD8, dual Ki-67/CD4$^{+}$ and Ki-67/CD8 staining in the pancreata of WT and *IRAK4*$^{fl/f}$ KPC mice. (*K*) FACS-based quantification comparing the percentage of peripheral blood CD8$^{+}$ T cells expressing high levels of intracellular TNF, IFNγ or IL-2 from WT and *IRAK4*$^{fl/f}$ KPC mice (N=6/arm). (*L*) FACS-based quantification of the percentage of intracellular TNF or IL-2 expressing CD8$^{+}$ T cell, the titers of these cytokines, and expression of exhaustion markers from WT and *IRAK4*$^{fl/f}$ KPC tumors (N=6/arm). For T cell subsets that express these cytokines, mean fluorescence intensity (MFI) was measured as levels of TNF and IFNγ expression. (*$P < .05$, **$P < .01$, ***$P < .001$, ****$P < .0001$ by ANOVA or two-tailed unpaired t-test; scale bars 50μM).

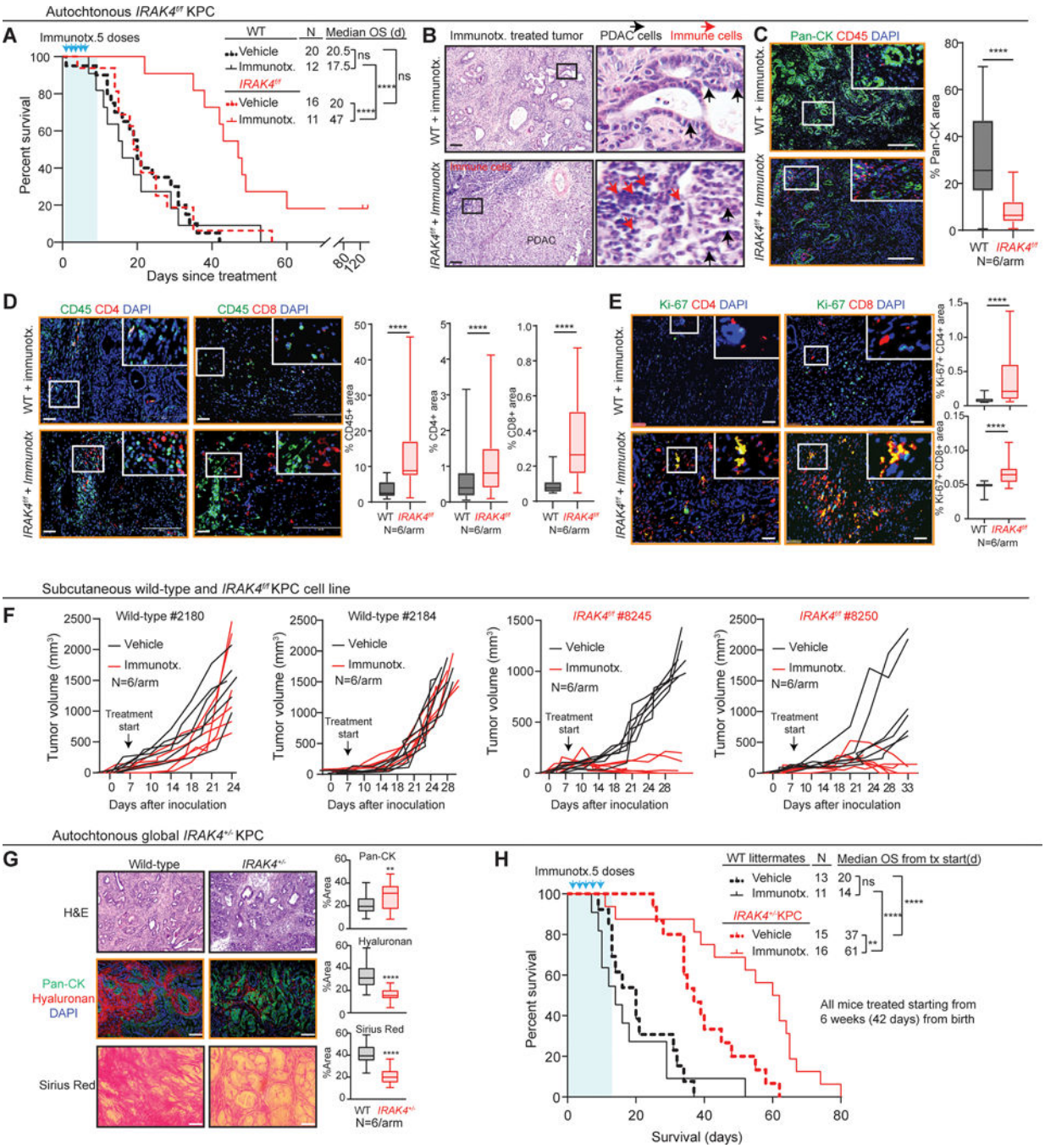


**Figure 6. Conditional *IRAK4*-deleted KPC mice respond to checkpoint immunotherapy.**

(*A*) Kaplan-Meier survival analysis of WT and *IRAK4*$^{fl/f}$ KPC mice treated with vehicle or immunotherapy (anti-CTLA4 plus anti-PD1) biweekly for 5 doses starting from six weeks of age. (*B*) Representative H&E pictures showing presence of abundant immune cells characterized by scant cytoplasm and prominent blue round nuclei in *IRAK4*$^{fl/f}$, but not WT, KPC tumors treated with immunotherapy. (*C-E*) Representative co-IF images and quantification showing reduced tumor burden (pan-CK area), increased infiltrative CD45$^{+}$ leukocytes, CD4$^{+}$ T cells, CD8$^{+}$ T cells, dual Ki-67$^{+}$CD4$^{+}$ T cells and Ki-67$^{+}$CD8$^{+}$

T cells in end-staged *IRAK4*$^{fl/f}$ KPC tumors compared to WT tumors treated with immunotherapy. (*F*) Growth kinetics of the indicated WT or *IRAK4*$^{fl/f}$ KPC cell lines (two each) grown subcutaneously in syngeneic C57BL/6J (six each) and treated with vehicle or immunotherapy biweekly for five doses. (*G*) Representative H&E, co-IF and Sirius red images, and quantification of Pan-CK, hyaluronan and Sirius red areas of end-staged tumors from WT and global heterozygous *IRAK4*$^{+/-}$ KPC littermates euthanized at humane endpoints (N=6/arm, 5–7 random 200X fields were used for analysis by ImageJ). (*H*) Kaplan-Meier survival analysis of WT and global heterozygous *IRAK4*$^{+/-}$ KPC littermates treated with vehicle or immunotherapy (anti-CTLA4 plus anti-PD1) biweekly for five doses starting from six weeks of age. (*$P < .05$, **$P < .01$, ***$P < .001$, ****$P < .0001$ by ANOVA or two-tailed unpaired t-test; scale bars 50μM).

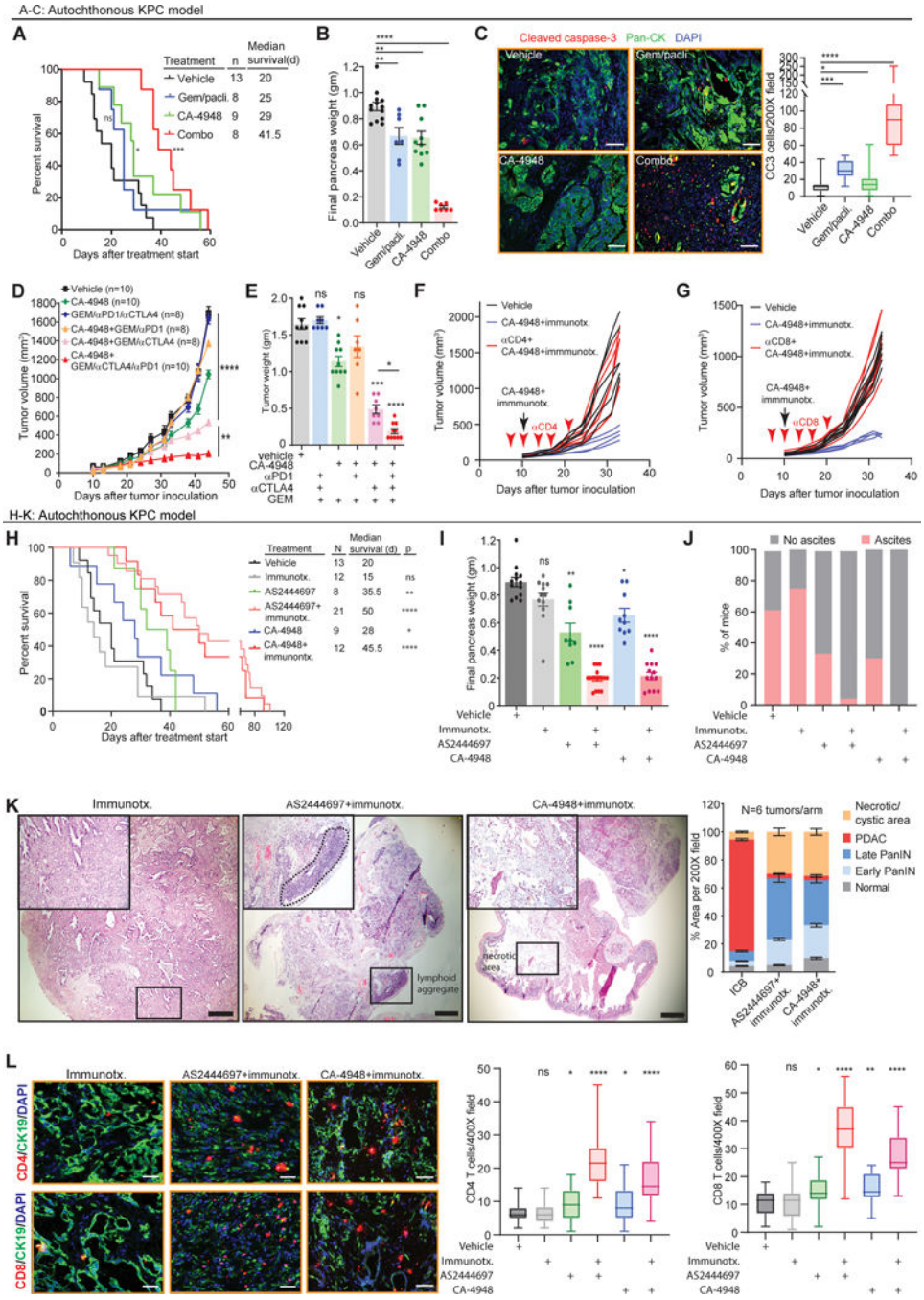


**Figure 7. Preclinical efficacy of IRAK4 inhibitor-based therapeutic strategies in PDAC.**

(*A*) Kaplan-Meier survival analysis and (*B*) final weights of the pancreata of KPC mice treated as indicated starting from six weeks of age until humane endpoints. (*C*) Representative co-IF images and quantification of Pan-CK$^+$ and cleaved caspase-3$^+$ cells in KPC tumors from different treatment arms. (*D, E*) Growth kinetics and final tumor weights of KI tumors grown subcutaneously in syngeneic FVB/NJ mice and treated as indicated. (*F, G*) Growth kinetics of individual KI tumors grown in FVB/NJ mice treated with vehicle or CA-4948+anti-CTLA4+anti-PD-1 without and with concurrent neutralizing anti-CD4$^+$ or

anti-$CD8^+$ antibodies intended to deplete $CD4^+$ or $CD8^+$ T cells, respectively (N=4–6/arm). (*H*) Kaplan-Meier analysis, (*I*) final pancreas weights and (*J*) ascites status of end-staged KPC mice treated with as indicated. (*K*) Representative H&E pictures and histopathologic quantification of end-stage pancreata from KPC mice treated as indicated. Highlighted areas were lymphoid aggregate or necrotic area identified by pathologist MBR. (*L*) Representative co-IF images of CK19 (green), and $CD4^+$ or $CD8^+$ (red), and quantification of $CD4^+$ or $CD8^+$ T cells in the indicated pancreata of end-staged KPC mice treated as indicated. (**P* < .05, ***P* < .01, ****P* < .001, *****P* < .0001 by ANOVA or two-tailed unpaired t-test, *L*: scale bars 50μM, *K*: scale bars 500μM).